# Chapter 22
# Engineering Upconversion Nanoparticles for Biomedical Imaging and Therapy

**Feng Chen, Wenbo Bu, Weibo Cai and Jianlin Shi**

## 22.1 Introduction

Upconversion nanoparticle (UCNP) has gained growing interests owing to their unique upconversion luminescence (UCL) features that are highly suitable for multimodal imaging in living subjects [1]. UCL is a unique process where low-energy continuous wave (CW) of near infrared (NIR) light is converted to higher energy light (emission bands ranging from ultraviolet [UV] to NIR region) through the sequential absorption of multiple photons or energy transfer [2]. After excitation using a 980 nm laser, UCNP could exhibit attractive optical features such as sharp emission lines [3], long lifetimes ($\sim$ms) [4], large anti-Stokes shift [3], superior photostability [5], high detection sensitivity [6], nonblinking and nonbleaching [5, 7], high tissue penetration depth [8], minimal photodamage [9], and extremely low auto-fluorescence [10]. Moreover, by doping with well-selected lanthanide ions of $Gd^{3+}$, $Er^{3+}/Yb^{3+}$ and $Tm^{3+}/Yb^{3+}$ (or combination of these ions) in suitable crystal hosts (e.g., $NaYF_4$), magnetic resonance (MR) and multicolor UCL imaging could be readily achieved [7, 11–13]. With the presence of heavy metal ions like $Gd^{3+}$, $Yb^{3+}$, and $Lu^{3+}$ in $NaYF_4$ matrix, such UCNP has also be considered as an intrinsic computed tomography (CT) contrast agent recently [14–16]. Importantly, in comparison with traditional optical imaging agents, such as organic dyes and quantum dots (QDs), UCNP excludes the potential UV photodamage and has low imaging background, high tissue penetration depth, and relatively low toxicity [1, 17].

F. Chen · W. Bu · J. Shi (✉)
State Key Laboratory of High Performance Ceramics and Superfine Microstructure, Shanghai Institute of Ceramics, Chinese Academy of Sciences, Shanghai 200050, People's Republic of China
e-mail: jlshi@mail.sic.ac.cn

W. Bu
e-mail: wbbu@mail.sic.ac.cn

W. Cai
Departments of Radiology, University of Wisconsin, Madison, Wisconsin, USA

W. Cai (ed.), *Engineering in Translational Medicine*,
DOI: 10.1007/978-1-4471-4372-7_22, 

Besides using UCNP as molecular imaging agents, loading UCNP with certain anticancer drugs (e.g., doxorubicin [DOX]) or photosensitizers (PSs) could further render attractive imaging-integrated chemotherapy or improved photodynamic therapy [18, 19]. All of these have made UCNP one of the most promising nanoparticles for future cancer imaging and therapy.

Here, we summarized the recent advances in engineering of UCNP for controlled size and morphology, tunable optical and surface properties, well-designed multiple imaging modalities, and integrated therapeutic functionality. Particle size, shape, surface properties, optical features of UCNP are extremely important for biological applications. The traditional synthetic strategies for the synthesis and surface modifications of high-quality UCNP will be briefly covered with our focus on some newly developed strategies for synthesizing ultrasmall UCNP with excellent upconversion property. Particularly, progress in engineering of UCNPs as multimodal molecular imaging probes will be reviewed in detail. We will also describe a few successful examples of in vitro and in vivo cancer therapy by using UCNP-based theranostic agents. Finally, we will discuss the present obstacles and future research directions in engineering of UCNP for biological imaging and therapy.

## 22.2 Engineering the Size and Morphology of UCNP

Uniform size and suitable morphology of UCNP could play a significant role in biological applications. So far, control and synthesis of UCNPs with tunable size (from sub-10 to over 100 nm) and various morphologies (such as nanospheres, nanocubes, nanorods, and nanoplates) have already been well-documented and are on longer a big challenge [1]. Oleic acid-assisted hydrothermal reaction and thermal decomposition are two of the most popular methods for the synthesis of various kinds of UCNPs with controlled size and morphology [20–22]. Recently, a user-friendly solvo thermal method has also been developed and been accepted as the most adopted strategy for not only single UCNP cores but core@multi-shell high-quality hexagonal-phase UCNPs [23, 24]. In this section, we focus our interest in reviewing newly developed strategies for synthesizing small UCNP with excellent UC properties.

Ultrasmall nanoparticle (<10 nm) with suitable surface modifications could become an attractive imaging probe which could not only target to tumor in vivo, but also potentially be cleared from kidney within reasonable time [25, 26]. Recent research showed that the absolute quantum yield (QY) of UCNP is relatively low and size-dependent [27]. Typically, 100 nm-sized UCNP could have a QY of about 0.3 %, and owing to the significantly increased surface defects in these ultrasmall UCNPs, it would suffer from a significant decrease to 0.005 % after decreasing the size down to $\sim$10 nm [27].

Wang et al. have offered an interesting solution by introducing the co-doping of gadolinium ($Gd^{3+}$) ions in $NaYF_4$:Er/Yb nanocrystals [28]. They demonstrated theoretically and experimentally that doping $NaYF_4$:Er/Yb with defined amount of $Gd^{3+}$ ion could simultaneously allow precise control over the phase (from cubic to

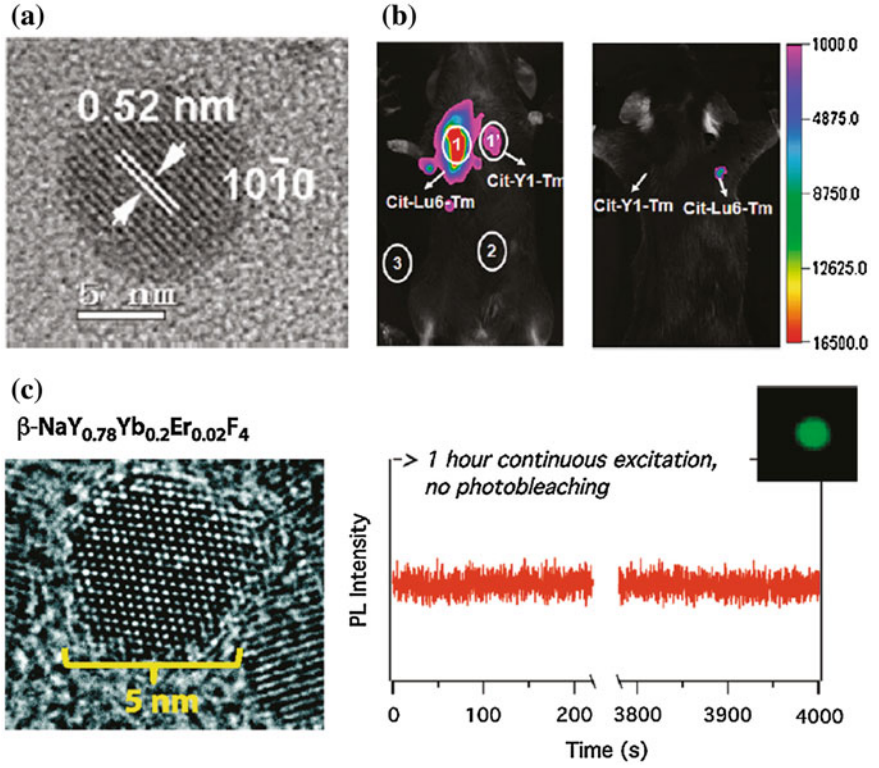


**Fig. 22.1** **a** TEM image of ~8 nm-sized $\beta$-$NaLuF_4$:Gd/Yb/Tm. **b** In vivo imaging of a black mouse after subcutaneous injection of citric acid-modified sub-10 nm-sized $\beta$-$NaLuF_4$:$Gd^{3+}$/$Yb^{3+}$/$Tm^{3+}$ and citric acid-modified $\beta$-$NaYF_4$:Yb/Tm when detected from the chest side (*left*) or the back side (*right*). **c** *Left* TEM image of $\beta$-$NaYF_4$:Yb/Er. *Right* The time trace of emission intensity from a single UCNP under continuous laser illumination for over 1 h (Recreated with kind permission of American Chemical Society [29, 46])

hexagonal), size (down to sub-10 nm), and UCL efficiency [28]. Inspired by this work, Liu et al. reported a greatly enhanced UCL efficiency in ~8 nm-sized $\beta$-$NaLuF_4$:Gd/Yb/Tm nanocrystals simply by replacing crystal host of $NaYF_4$ for $NaLuF_4$ (Fig. 22.1a) [29]. As-synthesized ultrasmall UCNP displayed bright UCL with a QY estimated to be $0.47 \pm 0.06$ %, which is even higher than the previously reported 100 nm-sized $NaYF_4$:Er/Yb (QY = $0.3 \pm 0.1$ %) [27]. The authors have further demonstrated an impressive in vivo deep tissue imaging (Fig. 22.1b) and attributed such greatly enhanced UCL in small UCNPs to the presence of hexagonal phase and successful suppression of nonradiative processes.

Besides improving the optical property of small UCNP either by altering the doping strategy or changing the crystal hosts, epitaxial growth of a protective shell represents the second technique for reducing the surface defects and improving the UCL property [30, 31]. However, successful synthesis of sub-10 nm-sized

core@shell-structured UCNP has not been achieved until very recently. By changing the concentration of basic surfactants, $Y^{3+}$:$F^{-}$ ratio and reaction temperature, Ostrowski et al. have succeeded in synthesizing core@shell-structured hexagonal-phase $NaYF_4$:Yb/Er@$NaYF_4$ with a diameter less than 10 nm [32]. As-synthesized smaller UCNP were extremely stable and exhibited no measurable photobleaching or blinking (Fig. 22.1c).

Although, the engineering of ultrasmall UCNPs for biological imaging and therapy is still at its early stage, they are expected to play a vital role in designing tumor-targeted imaging probe that could be efficiently cleared from body. To date, most of researchers are still interested in developing core@shell-structured UCNPs with particle size ranging from 10 to 50 nm for biological imaging applications.

## 22.3 Engineering of UCNP for Biological Imaging

### *22.3.1 Engineering the Surface for Water-Soluble UCNPs*

With the superior UCL properties and suitable surface modification and functionalization, UCNP has been demonstrated as a promising candidate of traditional imaging agents (e.g., QDs and organic dyes). Surface engineering is the first and a vital step before any biological imaging of UCNP. Although oleic acid-assisted strategy could guarantee high-quality UCNPs with uniform size and morphology, as-synthesized UCNPs are always coated with a layer of oleic acid ligands, which makes UCNPs water insoluble. So far methods used for engineering water-soluble UCNPs include ligand exchange (or removal) [33, 34], ligand oxidation reaction [35], layer-by-layer method [36], hydrophobic–hydrophobic interaction [37], host–guest interaction [38], and silanization [39].

### *22.3.2 Homemade In Vivo Imaging System for UCNP*

One of the obstacles in developing UCNP for biological imaging applications lies in the lack of 980 nm excitation source in nearly all of the commercially available confocal microscopes and in vivo imaging systems. To date, all of the in vitro and in vivo UCNP imaging researches are completed by using homemade (or modified) imaging systems [5, 6, 40].

Nyk et al. reported the first whole-body in vivo imaging of UCNP in mouse [40]. As-synthesized UCNPs (i.e., $NaYF_4$:Tm/Yb) were excited at 975 nm by a defocused emission from a fiber-coupled laser diode. An emission filter (cut off at 850 nm) was used to keep the 975 nm excitation light of the imaging CCD camera. Images were collected and processed by using Maestro GNIR FLEX fluorescence imaging system (CRi). After dosing the Balb-c mouse with

$NaYF_4$:Tm/Yb (200 μL of 2 mg/mL in water with 5 % glucose), a high-contrast signal from UCNPs could successfully be detected both through the skin and after dissection of the animal (Fig. 22.2a).

In a separated study, Xiong et al. reported an improved UCNP in vivo imaging setup by adding two CW 980 nm lasers, Andor DU897 EMCCD and filters to a Kodak in vivo imaging system [10]. The successful in vivo UCNP imaging has been demonstrated in U87MG and MCF-7 tumors bearing nude mice. After intravenous (i.v.) injection of RGD-labeled $NaYF_4$:Er/Tm/Yb ($\sim$50 μg/mouse), the mice were illuminated with two beam-expanded 980 nm lasers. A cooled EMCCD camera was then used to record the 800 nm emission of UCNPs and images were processed using Kodak molecular imaging software. As shown in Fig. 22.2b, under excitation of 980 nm laser, intense UCL signal could be observed in the U87MG tumor, while no significant signal could be seen in the MCF-7 tumor, indicating the targeted tumor uptake of UCNPs in U87MG. A high signal-to-noise ($\sim$24) between tumor and the background has been achieved in this study.

Besides modifying commercially available in vivo imaging systems by adding extra 980 nm laser and suitable filters, combining digital single-lens reflex (DSLR) camera and suitable optical filters might represent the simplest way to carry out an in vivo UCNP imaging experiment [41, 42]. Park et al. have built an in vivo UCNP imaging system by using a fiber-coupled 980 nm laser, a Nikon D90 DSLR camera, certain optical filters, and a dark box. The authors managed to image the tumor uptake of UCNP-Ce6 in nude mouse with their system [41]. Possibly because of the limited light coverage of 980 nm laser on mice, only signal from tumor site could be seen from the images (Fig. 22.2c). Also, since green light from UCNP could only have very limited tissue penetration depth, better in vivo images could be achieved by altering the system for detecting strong NIR (800 nm) or red (657 nm) emissions from UCNP.

### *22.3.3 Engineering of UCNP for Excellent NIR and Red Emissions*

#### 22.3.3.1 Strategies for Improving the NIR-Band Emission

Red and NIR light could have much deeper tissue penetration depth compared with UV and other visible light (e.g., blue and green light). Typically, UCL of UCNP is known to have multiple emission bands with various optical intensities after 980 nm excitation. For example, the emissions of $NaYF_4$:Er/Yb/Tm nanoparticles include UV (330–350 nm, 350–370 nm), blue (390–420 nm, 440–460 nm, 460–500 nm), green (510–530 nm, 530–570 nm), red (630–660 nm), and NIR (770–810 nm) bands [17]. Recently, there has been an increasing focus on the design and synthesis of UCNPs with tunable UC emission from UV to near-infrared (NIR) through

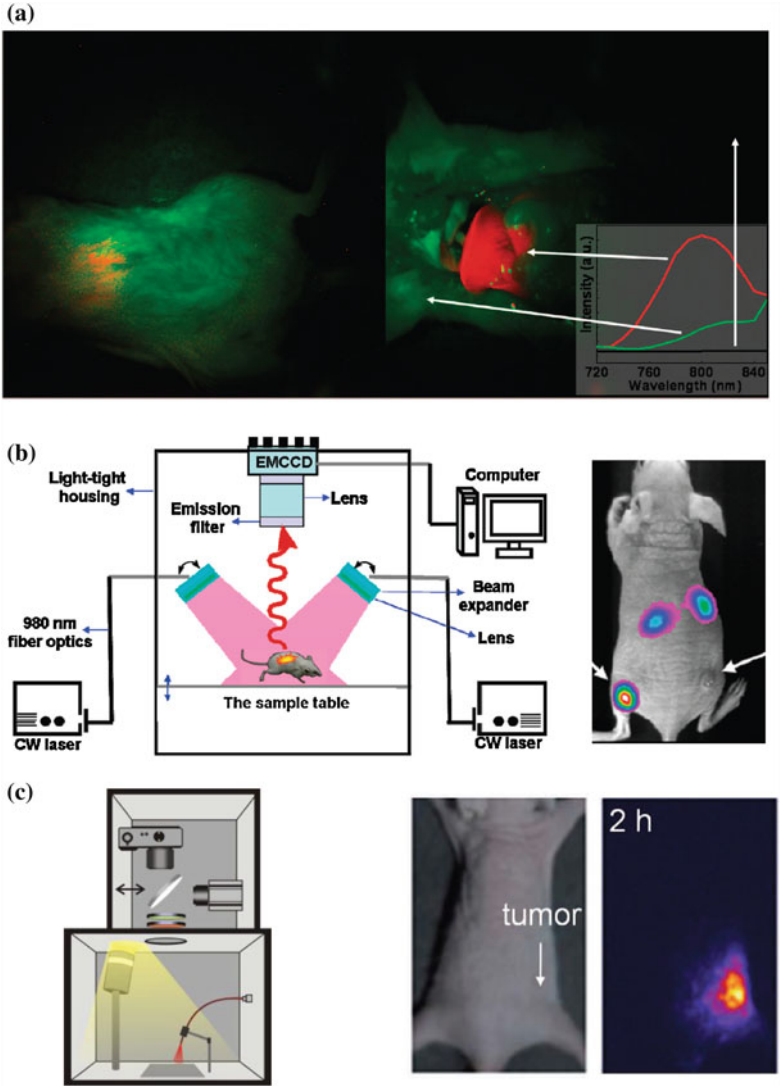


**Fig. 22.2** Comparison of different homemade UCNP in vivo imaging systems. **a** In vivo whole body images of mouse injected with UCNPs. Images were obtained in a modified Maestro GNIR FLEX fluorescence imaging system (CRi). (*left*) Intact mouse, (*right*) same mouse after dissection. **b** *Left* Schematic illustration of an in vivo UCNP imaging system based on modification of a Kodak in vivo imaging system. *Right* A representative images showing the in vivo tumor-targeted imaging of U87MG and MCF-7 tumors bearing mouse. **c** *Left* In vivo luminescence imaging setup which composed of a fiber-coupled 980 nm laser, a DSLR camera, optical filters, and a dark box. Middle: bright filed image of mouse. *Right* UCL image of the tumor site from mouse (Recreated with kind permission of American Chemical Society [10, 40] and Wiley–VCH Verlag GmbH & Co. KGaA [41])

various doping strategies or by introducing well-designed core@shell nanostructures [40, 43]. In particular, engineering of UCNPs with excellent NIR emission ($\lambda = \sim 800$ nm) or single-band red emission ($\lambda = \sim 650$ nm) could result in ideal optical biolabels for future deep tissue imaging and has become a new attractive topic currently [44].

The mostly used UCNP for achieving a NIR-to-NIR in vivo imaging is $Tm^{3+}$ and $Yb^{3+}$ co-doped $\beta$-$NaYF_4$, which, after 980 nm excitation, could give out strong NIR emission located at 800 nm, ideally for deep tissue imaging [8, 40]. Several interesting methods have been developed to improve the NIR emission intensity of $NaYF_4$:Tm/Yb nanoparticles.

Increasing the concentration of $Tm^{3+}$ ions in the host lattice is one of the simplest techniques to achieve the goal. Wang et al. demonstrated that $NaYF_4$:Tm/Yb nanoparticles with $Tm^{3+}$ doping fixed at 0.2 mol % could only have a weak emission at 800 nm, and increasing the $Tm^{3+}$ concentration up to 2 mol % could result in a significant enhancement thanks to the enhanced $^3H_4$ level [45]. By further replacing all $Y^{3+}$ in $NaYF_4$:Tm/Yb to $Yb^{3+}$ ions, Chen et al. have developed ultrasmall-sized (7–10 nm) $NaYbF_4$:Tm (2 mol %) nanoparticles with 3.6-fold enhancement in total upconversion emission intensity in comparison with that of 25 nm-sized $NaYF_4$:Tm/Yb (2/20 mol %) [46]. Such enhancement has been suggested to arise from the increased absorptions induced by the $Yb^{3+}$ ions and the increased efficiency of energy transfer between $Yb^{3+}$ and $Tm^{3+}$ ions. In a followed-up study, Liu et al. reported a lutetium (Lu)-based UCNP with excellent NIR emission [29]. As-synthesized sub-10 nm-sized $\beta$-$NaLuF_4$:Gd/Yb/Tm (24/20/1 mol %) displayed bright UCL with high QY estimated to be $0.47 \pm 0.06$ %. In comparison with 20 nm-sized $NaYF_4$:Tm/Yb (1/20 mol %), approximately 11-fold enhancement in NIR emission could be achieved. The successful suppression of nonradiative process has been suggested as the main reason behind such enhancement.

Epitaxial growth of an inert protective shell over pre-prepared $NaYF_4$:Tm/Yb core has been accepted as another useful strategy for minimizing the surface defects for preserving the optical integrity of UCNPs [30, 31]. Although cation-exchange and Ostwald ripening methods have been developed as alternative options recently [47, 48], seed-mediated growth still remains the most adopted technique for synthesis of such core@multi-shell structured UCNP [23]. By coating $\alpha$-$NaYbF_4$:Tm (0.5 mol %) with a well-selected $CaF_2$ protective shell, Chen et al. have developed a novel and biocompatible $\alpha$-$NaYbF_4$:Tm (0.5 mol %)/Yb@$CaF_2$ with highly efficient NIR-to-NIR upconversion property (Fig. 22.3a) [49]. $CaF_2$ was chosen as the epitaxial shell due to its low lattice mismatch with $\alpha$-$NaYbF_4$:Tm, good optical transparency, high crystallizability, stability, and biocompatibility. As-design UCNP exhibited an impressive high QY of $0.6 \pm 0.1$ % under low power density excitation (0.3 W/cm$^2$). Thanks to the suppressing of surface quenching effects via hetero-epitaxial growth of $CaF_2$ shell, an approximately 35-fold enhancement in UCL intensity could be achieved in comparison to the noncoated $\alpha$-$NaYbF_4$:Tm (Fig. 22.3b). The authors also demonstrated the possibility of imaging deep tissue by using $\alpha$-$NaYbF_4$:Tm(0.5 mol %)/Yb@$CaF_2$ nanoparticles. Clear NIR signal could be detected even through 3.2 cm pork tissue (Fig. 22.3c).

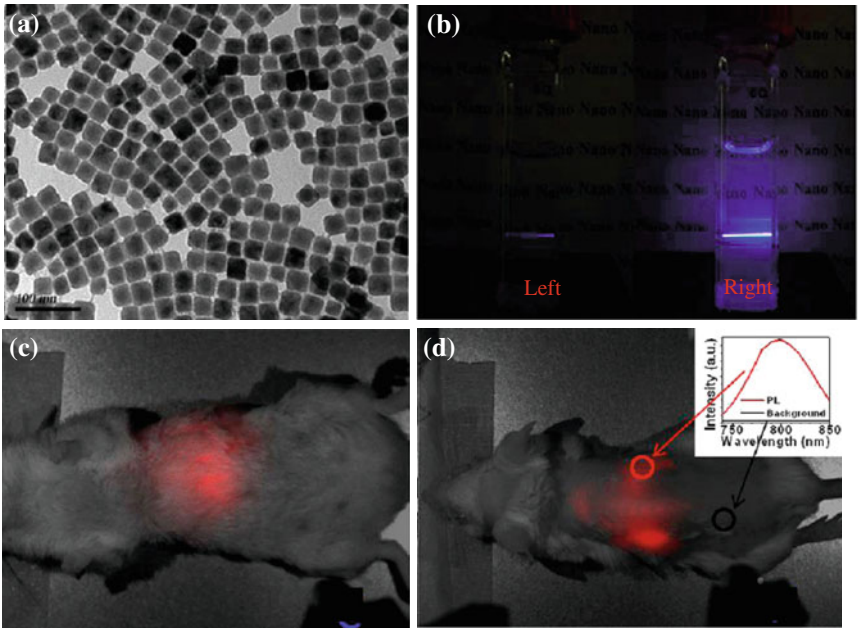


**Fig. 22.3** **a** TEM image of ~27 nm-sized α-$NaYbF_4$:Tm(0.5 mol %)/Yb@$CaF_2$. **b** Photographic images of cuvettes with suspensions of the core (*left*) and the core/shell (*right*) nanoparticles under laser excitation at 975 nm. Whole-animal imaging of a BALB/c mouse injected via tail vein with the HA-coated α-$NaYbF_4$:Tm(0.5 mol %)/Yb@$CaF_2$ core/shell nanoparticles. Mice were imaged in the **c** belly and **d** back positions. Insert in **d** is the spectra of the NIR upconversion luminescence and background taken from the circled area (Recreated with kind permission of American Chemical Society [49])

### 22.3.3.2 Strategies for Improving the Red-Band Emission

UCNP with strong single-band red emission has been emerged as another interesting imaging probe for in vivo imaging. Recently, studies on $Yb^{3+}/Er^{3+}$ co-doped $MnF_2$ and $KMnF_3$ nanoparticles have demonstrated a substantially enhanced red-to-green (R/G) emission ratio owing to the energy transfer between the $Er^{3+}$ and $Mn^{2+}$ [50, 51]. Inspired by these, Wang et al. have developed cube-shaped $KMnF_3$:Yb/Er (18/2 mol %) with extremely high red emission and completely disappeared blue and green emissions (Fig. 22.4a, b) [44]. Such single-band upconversion emission has been ascribed to nonradiative energy transfer from the $^1H_{9/2}$ and $^4S_{3/2}$ levels of $Er^{3+}$ to the $^4T_1$ level of $Mn^{2+}$, followed by back-energy transfer to the $^4F_{9/2}$ lever of $Er^{3+}$. Pure NIR emission of $KMnF_3$:Yb/Tm (18/2 mol %) could also be achieved by applying the same idea (Fig. 22.4c). In a followed-up study, Tian et al. presented a hydrothermal synthesis of $Mn^{2+}$-doped $NaYF_4$:Yb/Er nanoparticles with a strong single-band red emission [42].

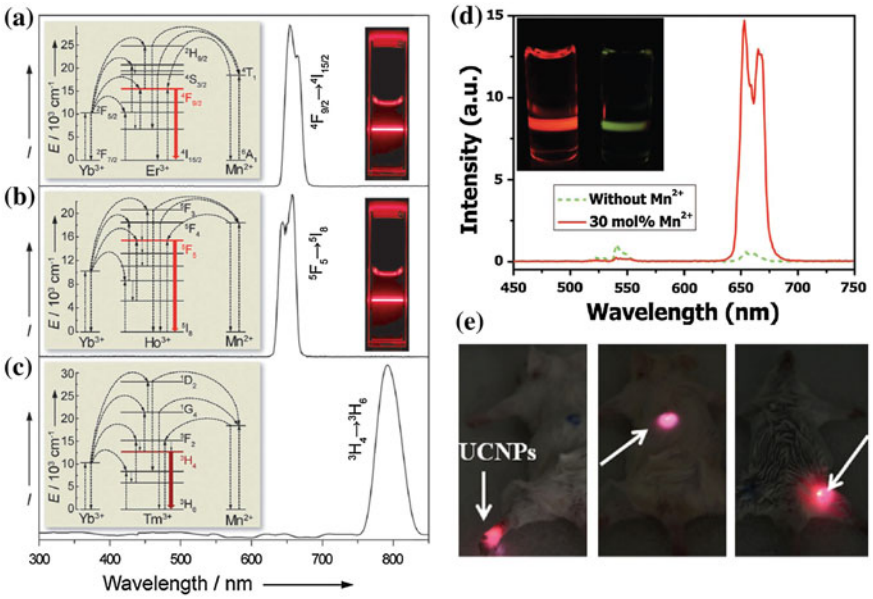


**Fig. 22.4** Room-temperature upconversion emission spectra of **a** $KMnF_3$:Yb/Er (18:2 mol %), **b** $KMnF_3$:Yb/Ho (18:2 mol %), and **c** $KMnF_3$:Yb/Tm (18:2 mol %) nanocrystals in cyclohexane (*insets* proposed energy transfer mechanisms and corresponding luminescent photos of the colloidal solutions). **d** Upconversion emission spectra of $NaYF_4$:Yb/Er (18/2 mol %) nanocrystals with 0 and 30 mol % $Mn^{2+}$ dopant ions dispersed in cyclohexane (1 mg/mL), respectively. (*inset* the corresponding luminescent photographs for intensity comparison). **e** In vivo upconversion luminescence imaging of PEG-UCNPs injected into translucent foot (*left*), skin of back (*middle*), and thin muscles of mice (*right*) (Recreated with kind permission of Wiley–VCH Verlag GmbH & Co. KGaA [42, 44])

Surprisingly, as-designed nanoparticles could have a R/G ratio of 163.78 after increasing the doping level of $Mn^{2+}$ up to 30 mol %. The doping of $Mn^{2+}$ also resulted in significant enhancement (about 15 times) in overall optical intensity in comparison with Mn-free sample (Fig. 22.4d). As a proof-of-concept experiment, the author injected water-soluble PEGylated $NaYF_4$:Yb/Er/Mn at the foot, back, and upper leg regions of white Kunming mice and demonstrated a clear tissue penetration and high-contrast photoluminescent imaging of the red emission (Fig. 22.4e).

The engineering of UCNP nanostructures for excellent NIR- and red-band emissions by doping with suitable amount of $Mn^{2+}$ ions will continue to attract increasing interests. More importantly, selectively doping UCNP with other lanthanide ions, such as $Gd^{3+}$, $Lu^{3+}$, $Yb^{3+}$, and $^{153}Sm^{3+}$ might endow UCNP with useful imaging modalities, such as magnetic resonance imaging (MRI), CT, and positron emission tomography (PET).

### 22.3.4 Engineering of UCNP for Multimodal Imaging

Each imaging modality has its strengths and weaknesses [52–55]. MRI provides excellent spatial resolution, exceptional anatomical information, and unlimited depth for in vivo imaging, but suffers from limited sensitivity. PET possesses remarkable detection sensitivity but only with a very limited spatial resolution (~mm). Photoluminescence imaging is capable of providing the highest spatial resolution and is the best modality for live cell imaging. However, it lacks the capability to obtain anatomical and physiological detail in vivo owing to limited penetration of light in tissues. Engineering of UCNP by suitable doping strategy could have a great possibility to achieve a multimodal imaging probe which holds balance in sensitivity, resolution, and penetration depth, enabling excellent visualizing (cancer) cells from the cellular scale to whole-body noninvasive imaging. In this section, we review the recent progress on how to engineer UCNP for in vivo multimodal imaging by lanthanide ions doping strategy.

#### 22.3.4.1 Engineering of UCNP for UCL/MR Dual-modal Imaging

Although combination of super paramagnatic iron oxide nanoparticles (SPIONs) with UCNP could result in bimodal imaging probe with UCL and MR modalities [39, 56], doping paramagnetic $Gd^{3+}$ ions (or $Mn^{2+}$) in UCNP crystal lattice should represent a better strategy for introducing MR contrast imaging capability without sacrificing the UCL intensities [11, 12]. Kumar et al. reported the first such example by doping $Gd^{3+}$ ions into $NaYF_4$ and demonstrated the combination of UCL and MR bimodal imaging in one single nanocrystal [12]. The first in vivo demonstration of such bimodal UCL/MRI imaging was later achieved using hexagonal-phase carboxylic acid-functionalized $NaGdF_4$:$Tm^{3+}$/$Er^{3+}$/$Yb^{3+}$ nanoparticles [13]. However, because the majority of the $Gd^{3+}$ ions are doped into the rigid crystal lattice and have limited chance to alter the relaxation time of surrounding water protons, only low MR sensitivity could be achieved in most of the previous reports [7, 12, 57]. The nanostructure re-engineering and relaxivity mechanism probing of the $Gd^{3+}$-doped UCNP might hold a great chance to enhance its MR sensitivity.

Recently, we have designed three different types of $Gd^{3+}$-doped UCNPs with various $Gd^{3+}$ ion locations and surface densities to probe the roles of surface and bulk $Gd^{3+}$ ions on shortening the $T_1$-relaxation time of surrounding water molecules [11]. Our systematic research have demonstrated that it is only the surface $Gd^{3+}$ ions in $Gd^{3+}$-doped UCNP are responsible for shortening the $T_1$-relaxation time of water protons, and bulk $Gd^{3+}$ ions could have little impact even with high concentration (Fig. 22.5). A remarkable increase in $r_1$-relaxivity (up to 6.18 $mM^{-1}s^{-1}/Gd^{3+}$) has been achieved by further decreasing the $NaGdF_4$ shell thickness down to <1 nm [11]. By using ultrasmall $NaGdF_4$ nanocrystals as models, Johnson et al. have shown the similar observation of increased $r_1$-

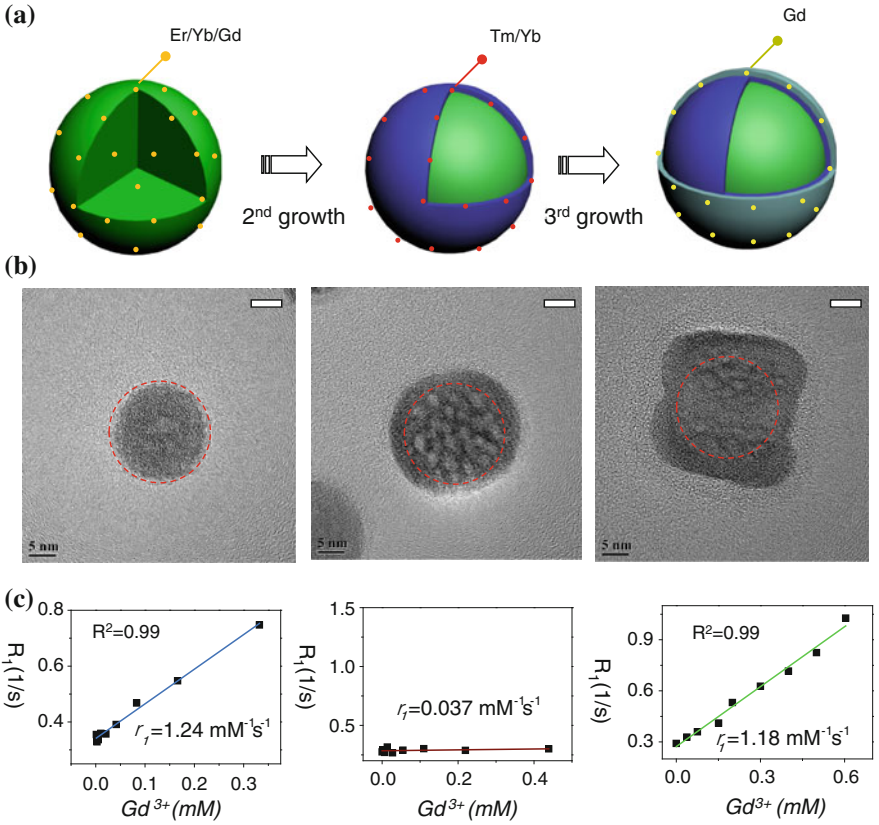


**Fig. 22.5** **a** A schematic illustration showing the synthesis of core@multi-shell UCNPs. **b** HR-TEM images of highly crystalline $NaYF_4$:Er/Yb/Gd (*left*), $NaYF_4$:Er/Yb/Gd@$NaYF_4$:Tm/Yb (*middle*), $NaYF_4$:Er/Yb/Gd@$NaYF_4$:Tm/Yb@$NaGdF_4$ (*right*) nanoparticles. **c** Plots of longitudinal relaxation rate ($R_1$) versus $Gd^{3+}$ concentration of three samples, (*left*) $NaYF_4$:Er/Yb/Gd@$SiO_2$ ($r_1 = 1.24\ mM^{-1}s^{-1}$), (*middle*) $NaYF_4$:Er/Yb/Gd@$NaYF_4$:Tm/Yb@$SiO_2$ ($r_1 = 0.037\ mM^{-1}s^{-1}$), and (*right*) $NaYF_4$:Er/Yb/Gd@$NaYF_4$:Tm/Yb@$NaGdF_4$@$SiO_2$ ($r_1 = 1.18\ mM^{-1}s^{-1}$) (Recreated with kind permission of Wiley–VCH Verlag GmbH & Co. KGaA [11])

relaxivity per $Gd^{3+}$ ion (from 3.0 to 7.2 $mM^{-1}s^{-1}$) with decreased $NaGdF_4$ particle size (from 8 to 2.5 nm), again demonstrating the role of surface $Gd^{3+}$ ions in relaxivity enhancement [58].

In an attempt to understand the relaxivity mechanism of $Gd^{3+}$-doped UCNP, we further introduced mesoporous and dense silica coatings for systematically investigating its possible relaxivity mechanisms [59]. A surface-dependent relaxivity mechanism has been proposed based on our results. Specifically, we showed a co-existing of inner- and outer-sphere $r_1$-relaxivity mechanism in ligand-free $Gd^{3+}$-doped UCNP, while only main contribution of outer-sphere mechanism in silica-shielded probes. The origin of $r_2$-relaxivity is inferred mainly from an outsphere mechanism with the $r_2$ value being surface state related. Also, key factors

for tuning $r_2/r_1$ ratio have been found to be highly dependent on the thickness of $NaGdF_4$ shell and surface modification strategy. Based on these, we showed a 105-fold enhancement in $r_1$-relaxivity (14.73 $mM^{-1}s^{-1}/Gd^{3+}$) in comparison with the first-reported same value (0.14 $mM^{-1}s^{-1}/Gd^{3+}$). These new findings provide not only deeper insight into the origin of contrast enhancement of water-soluble $Gd^{3+}$-doped UCNP, but also useful strategy for achieving both high MR sensitivity for future biological imaging applications.

#### 22.3.4.2 Engineering of UCNP for UCL/MR/CT Triple-modal Imaging

With the presence of heavy metal ions like $Gd^{3+}$, $Yb^{3+}$, and $Lu^{3+}$ in $NaYF_4$ matrix, lanthanide ions-doped UCNPs also have been considered as an inherent CT contrast agent recently [14–16, 60]. Ultrasmall $NaGdF_4$:Er/Yb nanocrystals have firstly been developed via an interesting two-phase system and been demonstrated as UCL/MR/CT triple-modal imaging contrast agent [14]. In a followed-up study, Liu et al. reported a Yb-based $NaYbF_4$:Er/Gd nanoparticles with improved CT contrast capabilities [15]. The doping of $Gd^{3+}$ ions has been demonstrated vital to control both the morphology and R/G ratio of $NaYbF_4$:Er/Gd nanoparticles (Fig. 22.6a, b). As-synthesized water-soluble polyethylene glycol (PEG)-modified $NaYbF_4$:Er/Gd nanoparticles have been found to be the best CT contrast agents among iobitridol, Au-, Pt-, Bi-, and Ta-based nanoparticulate agents under the same testing conditions. In vivo imaging study demonstrated the capability of PEG-modified $NaYbF_4$:Er/Gd nanoparticles as an excellent CT contrast agent (Fig. 22.6c, d). Water-soluble $NaLuF_4$:Tm/Yb nanoparticles might represent the third type of inherent CT agents. After coating with iron oxide shell, or modified with $Gd^{3+}$-complex, such modified $NaLuF_4$:Tm/Yb nanoparticles could also be probes with well-combined UCL/MR/CT triple modalities [16, 61, 62]. Although other matrixes, such as $BaYbF_5$ and $BaGdF_5$ [63, 64], have also been reported as inherent CT contrast agents, they might not be a good choice for efficient up-conversion optical imaging.

Another way for adding a CT contrast capability is by decorating $Gd^{3+}$ ions-doped UCNP with CT contrast nanoparticles, such as tantalum oxide ($TaO_x$) and ultrasmall gold nanoparticles (Fig. 22.7) [60, 65]. Starting from $NaYF_4$:Yb/Er/Tm@$NaGdF_4$ nanocrystals, we recently demonstrated an efficiently way to add CT imaging modality by decorating with a fluorescence-transparent $TaO_x$ shell [65]. As-design water-soluble litchi-shaped trimodal imaging probe showed an extraordinary high $r_1$ (11.45 $mM^{-1}s^{-1}$) and $r_2$ (147.3 $mM^{-1}s^{-1}$) values thanks to the ultrathin $NaGdF_4$ shell. An obvious CT contrast enhancement could be obtained by the combined effect of radiopaque $TaO_x$ shell and UCNP itself. Both the in vitro and in vivo trimodal imaging have been demonstrated, providing us a new possibility for potential early cancer detection.

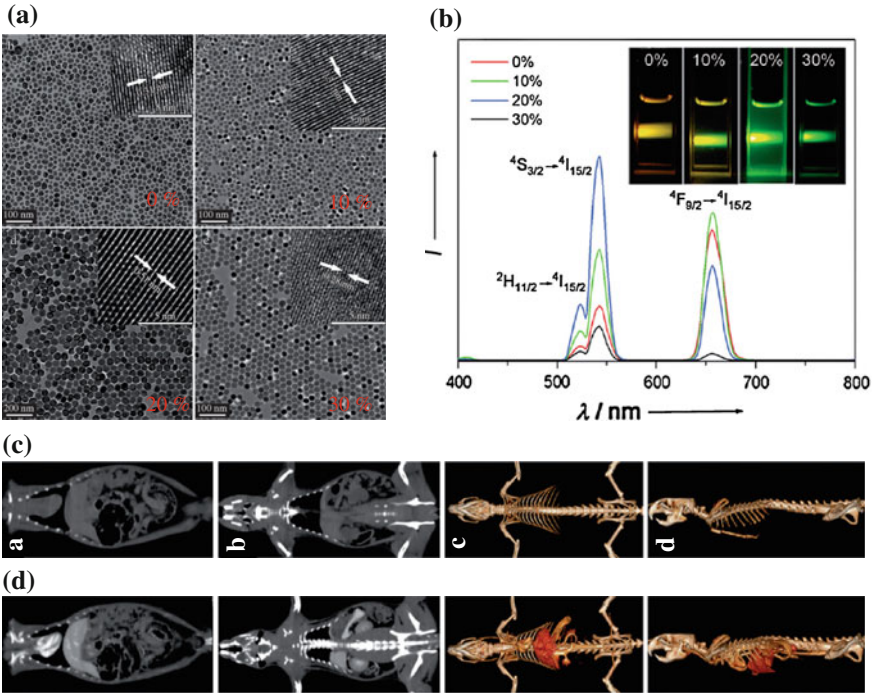


**Fig. 22.6** **a** TEM image of Gd-doped $NaYbF_4$:Er nanoparticles with various doping levels of $Gd^{3+}$ ions and corresponding **b** room temperature NIR-to-Vis upconversion luminescence spectra. The inset in **b** shows the upconversion luminescence photograph of the Gd-doped $NaYbF_4$:Er nanoparticles with different concentrations of Gd under excitation at 980 nm. In vivo CT coronal view images of a rat after intravenous injection of 1 mL PEG-UCNPs (70 mgYb/mL) solution at different time intervals. **c** Pre-injection, **d** 10 min postinjection (Recreated with kind permission of Wiley–VCH Verlag GmbH & Co. KGaA [15])

### 22.3.4.3 Engineering of Radiolabeled UCNP for PET/SPECT Imaging

Suitable surface engineering and isotopes labeling of UCNP could make it also a PET/SPECT (i.e. single-photon emission computed tomography) tracer. To date, research on synthesis and application of radioactive UCNP (*r*-UCNP) is still in its infancy. Two techniques have been developed for the synthesis of radioactive UCNP. They are surface ion reaction (or exchange) method and direct isotope(s) doping strategy.

$^{18}$F-labeled UCNP, synthesized via surface ion reaction between $^{18}$F and rare-earth ions, is the first-reported *r*-UCNP [66–69]. Simply by incubating $^{18}$F ions with nanoparticles that contain rare-earth ions [e.g., $Y_2O_3$, $NaYF_4$, $NaYF_4$:Yb/Tm, $Y(OH)_3$ and $Gd(OH)_3$], researchers from Li's group have demonstrated that the labeling of $^{18}$F can be achieved impressively with an average yield of >90 % within only one minute [67]. The effectiveness of $^{18}$F-labeled rare-earth nanoparticles was further evaluated by PET imaging of their in vivo distribution and

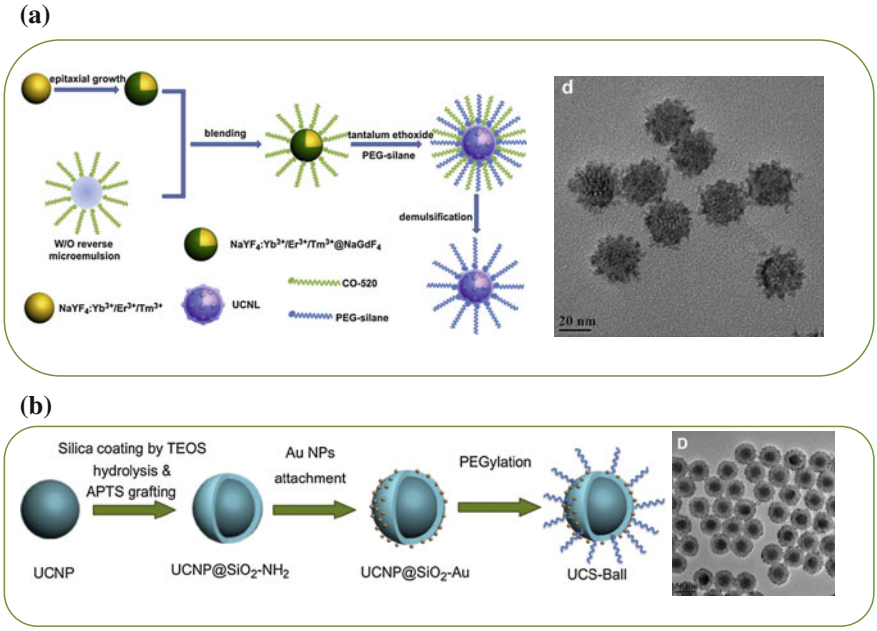


**Fig. 22.7** Schematic illustration and TEM image of **a** $TaO_x$-decorated $NaYF_4$:Yb/Er/Tm@NaGdF$_4$ nanoparticles, **b** gold nanoparticles-decorated $NaYF_4$:Yb/Er/Tm/Gd (Recreated with kind permission of Elsevier [60, 65])

application in lymph monitoring (Fig. 22.8). The same group later demonstrated that radioactive $^{153}Sm^{3+}$ could also be embedded into the UCNP matrix via a cation-exchange process, resulting in $^{153}$Sm-labeled $NaLuF_4$:Yb/Gd/Tm [70].

Simply by reacting slight amount of $^{153}SmCl_3$ with other normal precursors (e.g., oleic acid, sodium oleate, $LuCl_3$, $YbCl_3$ and $TmCl_3$) at 160 °C for 8 h, Li's group also reported a one-pot hydrothermal synthesis of $NaLuF_4$:$^{153}$Sm/Yb/Tm nanocrystals as UCL/SPECT bimodal imaging agent [71]. Their results showed that the introduction of small amount of radioactive $^{153}Sm^{3+}$ showed little influence on the upconversion luminescence properties. Lower cytotoxicity and excellent in vitro and in vivo performance have also been demonstrated by using UCL/SPECT dual imaging modalities. Since $NaLuF_4$ nanoparticles have already been demonstrated as an excellent CT contrast agent [16, 61], and doping $Gd^{3+}$ could not only enhance the UCL intensity of $NaLuF_4$:Tm/Yb, but also introduce MR imaging modality, water-soluble $NaLuF_4$:$^{153}$Sm/Gd/Tm/Yb nanoparticle might represent one of the best multimodal imaging probes so far.

Of note, the above-mentioned rapid and efficient labeling of rare-earth nanoparticles with $^{18}$F and $^{153}$Sm may not represent a general strategy for labeling other PET/SPECT isotopes such as $^{11}$C ($t_{1/2}$:20.4 min), $^{64}$Cu ($t_{1/2}$:12.7 h), $^{68}$Ga ($t_{1/2}$:67.7 min), $^{86}$Y ($t_{1/2}$:14.7 h), $^{89}$Zr ($t_{1/2}$:3.3 d), $^{124}$I ($t_{1/2}$:4.2 d), $^{99m}$Tc ($t_{1/2}$:6.0 h), $^{111}$In ($t_{1/2}$:2.8 d). Postisotope labeling with the assistance of

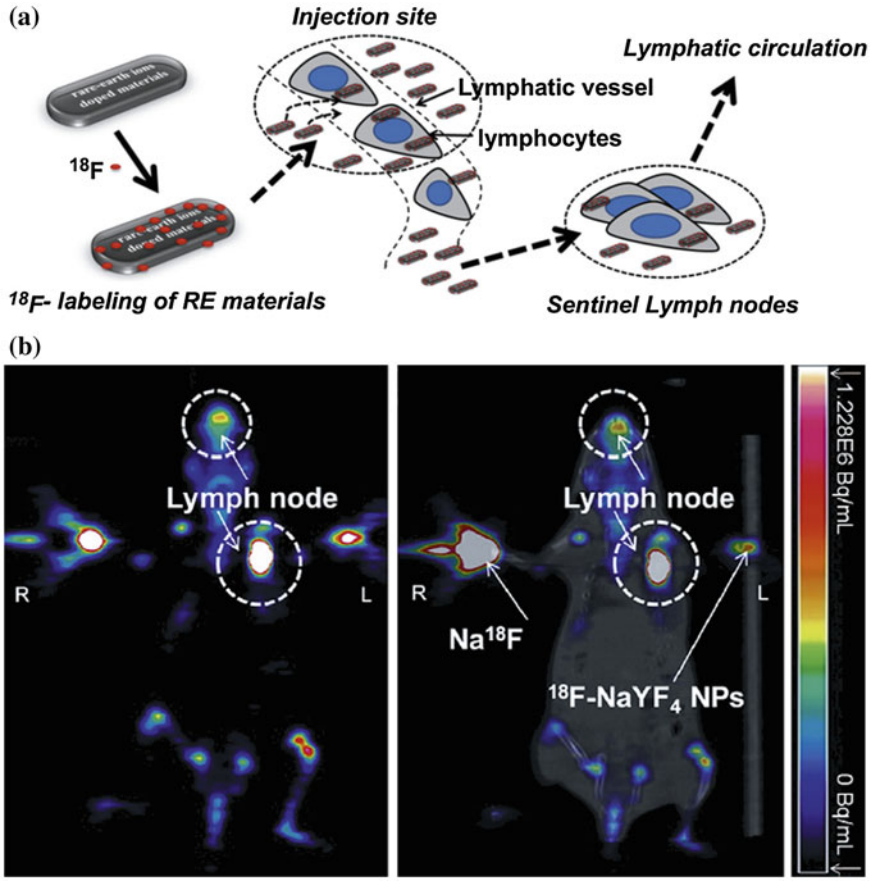


**Fig. 22.8** **a** Schematic representation of preparation of 18F-labeled rare-earth nanoparticles and lymph node imaging mechanism. **b** PET imaging (*left*) and PET/CT imaging (*right*) of lymph node 30 min after subcutaneous injection of $^{18}$F-UCNPs (Recreated with kind permission of Elsevier [67])

certain chelators should be the best choice for labeling many different kinds of radioactive metal ions.

Over 10 years of efforts in engineering of UCNP have made it a powerful imaging probe, which could also be a useful nanoplatform for integrating therapeutic capability. Although breakthrough in cancer-targeted imaging and therapy has not been achieved yet, developing of smart and efficient UCNP-based theranostic nanosystems has still attracted growing interests recently [18, 19].

### 22.3.5 Engineering of UCNP for Integrating Therapeutic Functionality

To date, only limited progress has been achieved in regard to using UCNP as a drug delivery vehicle. How to improve the drug-loading capacity and in vivo tumor-targeted drug delivery of such UCNP-based theranostic nanosystems are still two of most obvious obstacles in this field. In this section, we will review some examples on design, synthesis, and application of theranostic nanosystems based on UCNPs.

Generally, loading small molecular anticancer drugs and PSs into surface-modified UCNPs are two of the main strategies for integrating therapeutic functionality. Smart hydrogels [72], mesoporous silica shell [18, 19, 73], dense silica shell [74–76], amphiphilic copolymer [77, 78], chitosan [79], polyethylene glycol (PEG) or PEG-phospholipids [80, 81], and poly(ethylene)imine (PEI) [82] have already been used for not only transferring UCNPs into water phase, but also loading DOX and many different kinds of PSs into the systems.

Loading DOX into mesoporous or polymer-coated UCNP to form theranostic agents has been reported [18, 80, 83]. Zhang et al. have developed novel magnetic upconversion fluoride nanorattles via an ion-exchange process [18]. Small molecular drug of DOX could be loaded into the free volume of the nanorattles with a high loading capacity of 32 wt %. With the SPION and UCNP together in the system, in vivo UCL imaging has been used to demonstrate the accumulation of nanocarriers in tumor site when applying a magnetic field near the tumor site. In vivo therapeutic investigation in marine hepatocarcinoma (H22) tumor-bearing mice showed a significant inhibition of tumor growth rate after injecting DOX-loaded nanorattles while applying with a magnetic field (Fig. 22.9). In another study, magnetic-guided thermal therapeutic effect could also be integrated in a UCNP nanoplatform by engineering the UCNP surface with ultrasmall $Fe_3O_4$ and gold nanoparticles through a layer-by-layer strategy [84].

By using the visible emission bands of UCNP for triggering the generation of singlet oxygen, researchers have developed many different versions of UCNP/PS nanocomposites for 980 nm laser-initiated photodynamic therapy (PDT). Owing to the advantage in deeper tissue penetration depth of 980 nm in comparison with the traditional visible light, such UCNP/PS-based PDT agents should hold better potential for treating deeper cancer using PDT. Since the first report on UCNP/M540 (i.e., Merocyanine-540)-based PDT agent [76], many other combinations of UCNP/PS have been reported and the quest for strategies to improve the PDT efficiency is continuing [19, 41, 72–75, 78, 81, 82, 85].

The first prototype of UCNP/PS-based PDT drug was constructed by encapsulating M540 into a silica matrix using traditional Stöber method [76]. Due to the electrostatic repulsion between negatively charged M540 and the tetraethyl orthosilicate (TEOS) precursor, the loading capacity of M540 was limited. We recently reported a new UCNP/PS-based PDT drug by using brighter $Gd^{3+}$-doped

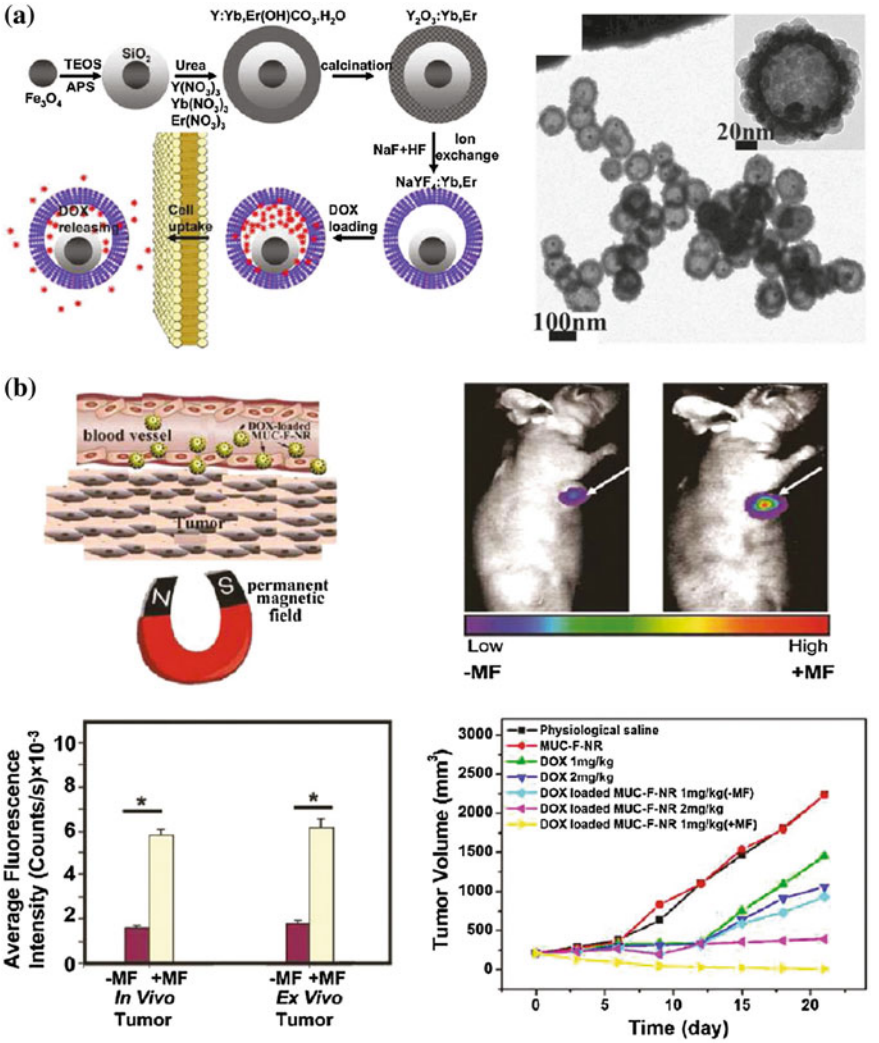


**Fig. 22.9** **a** Synthetic procedure for the drug-loaded $Fe_3O_4$@$SiO_2$@α-NaYF/Yb,Er nanorattles (*left*) and TEM image of $Fe_3O_4$@$SiO_2$@α-NaYF/Yb,Er (*right*). **b** In vivo magnetic-guided chemotherapy of $Fe_3O_4$@$SiO_2$@α-NaYF/Yb,Er (Recreated with kind permission of American Chemical Society [87])

UCNP and water-soluble methylene blue (MB) [75]. Successful "trapping" of the positively charged MB within the negatively charged silica resulted in a core@-shell structure of UCNP@$SiO_2$(MB) with attractive properties such as higher PS-loading capacity, zero-PS-prerelease, 980 nm laser on-demand $^1O_2$ release, and UCL/MR dual-modal imaging capabilities.

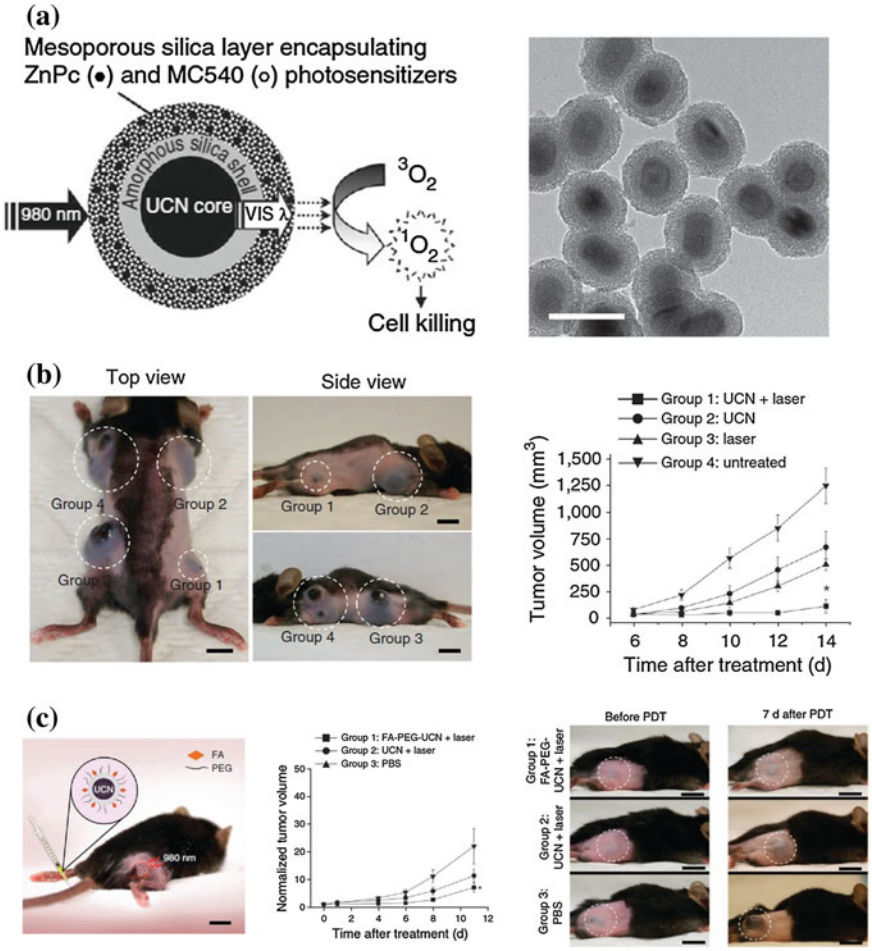


**Fig. 22.10** **a** Schematic of mesoporous-silica-coated UCNPs co-loaded with ZnPc and MC540 photosensitizers for PDT (*left*), and TEM image of mesoporous-silica-coated UCNPs (*right*). **b** In vivo PDT of injected tumor cells prelabeled with UCNPa. **c** Targeted in vivo PDT of a subcutaneous tumor model injected with FA-PEG-UCNPs (Recreated with kind permission of Nature Publishing Group [19])

Although many different kinds of UCNP/PS systems have been developed most of the therapeutic studies were only limited to in vitro studies mainly because of the relatively low efficiency of as-designed PDT agent. By carefully selecting and loading two or more different kinds PSs into the system, PSs are able to completely utilize the emission bands of UCNP. Such multiple-PS-loading strategy might hold a better chance for further enhancing the PDT effect. Idris et al. recently demonstrated this idea by encapsulating two different PSs (ZnPC and MC540) into mesoporous-silica-coated $NaYF_4$:Er/Yb nanoparticles (Fig. 22.10a) [19]. In vitro

experiments demonstrated the higher generation of singlet oxygen and lower cell viability when shedding 980 nm light on co-loaded nanoparticles. To demonstrate the in vivo PDT effect, they injected B10-F0 melanoma cell pre-labeled with double-PS-loaded UCNP under the skin of C57BL/6 mice and then irradiated the injected site with a 980 nm laser. Successful inhibit of tumor growth rate has been observed in the positive group, while only continuous tumor growth could be seen in the control groups (Fig. 22.10b). However, in the case of injecting the drug intratumorally and intravenously, only slightly tumor growth inhibition could be achieve, indicating that in vivo PDT effect is still limited (Fig. 22.10c). Since the half-life of singlet oxygen is very short, on the order of microseconds, and can therefore act only on target structures that are in close proximity to it, in order to guarantee an effective PDT therapeutic outcome, sufficient amount of PDT agents should be able to internalize by the cells. Unfortunately, achieving this goal has long been considered as one of the biggest challenges in the war against cancer [86].

## 22.4 Conclusion and Future Perspectives

In conclusion, we summarized the very recent advances in engineering of UCNPs for cancer imaging and therapy applications. Engineering of ultrasmall-sized UCNP with excellent optical properties has attracted increasing interests and will potentially be used for designing a renal clearable UCNP-based imaging probe. Because of their advantages in imaging deeper tissue, UCNP with strong near-infrared emissions (or single red band) has also attracted growing interest recently. Doping suitable ions into UCNP crystal lattices has become one of the most unique and efficient techniques for integrating many clinical relevant imaging modalities (e.g., PET, MRI, SPECT, and CT) together in one single UCNP.

Despite recent progress in engineering of UCNP for tunable size and improve imaging capabilities, many challenges still remained for future cancer imaging and therapy of UCNP.

1. Improving the upconversion efficiency of ultrasmall UCNPs. Development and optimization of strategies for synthesis of ultrasmall UCNPs with high optical quality will be urgently needed in the coming years. Such UCNPs are expected to play a vital role in designing clinically translational tumor imaging probe which could targeted specifically to tumor and excreted through kidney within hours.
2. Perfection of NIR and red emission intensities of UCNPs. Owing to their high tissue penetration depth, UCNPs with excellent NIR emission or single-band red emission has been considered as the ideal probes for in vivo optical imaging applications. Strategies for further improving NIR- and red-band emission efficiency of UCNPs will become a new hot topic in this filed.

3. Developing imaging systems specifically for tracking UCNPs both in vitro and in vivo. Considering that most of the UCNP imaging systems are homemade by employing an additional 980 nm laser module, commercialization of in vivo imaging system which can be used for whole-body imaging of UCNP in small animals will be very helpful for speeding up the development and application of UCNPs.
4. Design of theranostic nanomedicines based on UCNP. So far, only small molecular anticancer drugs and photosensitizers have been loaded within surface-engineered UCNPs for simultaneous imaging and therapy. Although a few examples about integrated imaging and therapy have been reported, new strategies are still needed for achieving enhanced therapeutic efficiency.
5. Targeting UCNP to the tumor site. To date, in vivo tumor cell (or tumor vasculature) targeting based on UCNP is still a big challenge. Optimization of particle size, surface characteristics, as well as selecting the suitable targeting ligands to improve the targeting efficiency, should deserve more research efforts in the coming future.

## References

1. Zhou J, Liu Z, Li F (2012) Upconversion nanophosphors for small-animal imaging. Chem Soc Rev 41(3):1323–1349. doi:10.1039/c1cs15187h
2. Auzel F (2004) Upconversion and anti-Stokes processes with f and d ions in solids. Chem Rev 104(1):139–173. doi:10.1021/cr020357g
3. Haase M, Schafer H (2011) Upconverting nanoparticles. Angew Chem Int Ed 50(26):5808–5829. doi:10.1002/anie.201005159
4. Ju Q, Tu D, Liu Y, Li R, Zhu H, Chen J, Chen Z, Huang M, Chen X (2012) Amine-functionalized lanthanide-doped KGdF4 nanocrystals as potential optical/magnetic multimodal bioprobes. J Am Chem Soc 134(2):1323–1330. doi:10.1021/ja2102604
5. Wu S, Han G, Milliron DJ, Aloni S, Altoe V, Talapin DV, Cohen BE, Schuck PJ (2009) Non-blinking and photostable upconverted luminescence from single lanthanide-doped nanocrystals. Proc Natl Acad Sci U S A 106(27):10917–10921. doi:10.1073/pnas.0904792106
6. Cheng L, Wang C, Liu Z (2012) Upconversion nanoparticles and their composite nanostructures for biomedical imaging and cancer therapy. Nanoscale 5(1):23–37. doi:10.1039/c2nr32311g
7. Park YI, Kim JH, Lee KT, Jeon KS, Bin Na H, Yu JH, Kim HM, Lee N, Choi SH, Baik SI, Kim H, Park SP, Park BJ, Kim YW, Lee SH, Yoon SY, Song IC, Moon WK, Suh YD, Hyeon T (2009) Nonblinking and nonbleaching upconverting nanoparticles as an optical imaging nanoprobe and T1 magnetic resonance imaging contrast agent. Adv Mater 21 (44):4467. doi:10.1002/adma.200901356
8. Chatterjee DK, Rufaihah AJ, Zhang Y (2008) Upconversion fluorescence imaging of cells and small animals using lanthanide doped nanocrystals. Biomaterials 29(7):937–943. doi:10.1016/j.biomaterials.2007.10.051
9. Nam SH, Bae YM, Park YI, Kim JH, Kim HM, Choi JS, Lee KT, Hyeon T, Suh YD (2011) Long-term real-time tracking of lanthanide ion doped upconverting nanoparticles in living cells. Angew Chem Int Ed 50(27):6093–6097. doi:10.1002/anie.201007979

10. Xiong L, Chen Z, Tian Q, Cao T, Xu C, Li F (2009) High contrast upconversion luminescence targeted imaging in vivo using peptide-labeled nanophosphors. Anal Chem 81(21):8687–8694. doi:10.1021/ac901960d
11. Chen F, Bu WB, Zhang SJ, Liu XH, Liu JN, Xing HY, Xiao QF, Zhou LP, Peng WJ, Wang LZ, Shi JL (2011) Positive and negative lattice shielding effects co-existing in Gd(III) ion doped bifunctional upconversion nanoprobes. Adv Funct Mater 21(22):4285–4294. doi:10.1002/adfm.201101663
12. Kumar R, Nyk M, Ohulchanskyy TY, Flask CA, Prasad PN (2009) Combined optical and MR bioimaging using rare earth ion doped NaYF4 nanocrystals. Adv Funct Mater 19(6):853–859. doi:10.1002/adfm.200800765
13. Zhou J, Sun Y, Du X, Xiong L, Hu H, Li F (2010) Dual-modality in vivo imaging using rare-earth nanocrystals with near-infrared to near-infrared (NIR-to-NIR) upconversion luminescence and magnetic resonance properties. Biomaterials 31(12):3287–3295. doi:10.1016/j.biomaterials.2010.01.040
14. He M, Huang P, Zhang CL, Hu HY, Bao CC, Gao G, He R, Cui DX (2011) Dual phase-controlled synthesis of uniform lanthanide-doped NaGdF4 upconversion nanocrystals via an OA/Ionic Liquid Two-Phase System for in vivo dual-modality imaging. Adv Funct Mater 21(23):4470–4477. doi:10.1002/adfm.201101040
15. Liu Y, Ai K, Liu J, Yuan Q, He Y, Lu L (2012) A high-performance ytterbium-based nanoparticulate contrast agent for in vivo X-ray computed tomography imaging. Angew Chem Int Ed 51(6):1437–1442. doi:10.1002/anie.201106686
16. Zhu X, Zhou J, Chen M, Shi M, Feng W, Li F (2012) Core-shell Fe3O4@NaLuF4:Yb, Er/Tm nanostructure for MRI, CT and upconversion luminescence tri-modality imaging. Biomaterials 33(18):4618–4627. doi:10.1016/j.biomaterials.2012.03.007
17. Wang F, Banerjee D, Liu Y, Chen X, Liu X (2010) Upconversion nanoparticles in biological labeling, imaging, and therapy. Analyst 135(8):1839–1854. doi:10.1039/c0an00144a
18. Hong H, Yang K, Zhang Y, Engle JW, Feng L, Yang Y, Nayak TR, Goel S, Bean J, Theuer CP, Barnhart TE, Liu Z, Cai W (2012) In Vivo Targeting and Imaging of Tumor Vasculature with Radiolabeled, Antibody-Conjugated Nanographene. Acs Nano 6(3):2361–2370. doi:10.1021/nn204625e
19. Idris NM, Gnanasammandhan MK, Zhang J, Ho PC, Mahendran R, Zhang Y (2012) In vivo photodynamic therapy using upconversion nanoparticles as remote-controlled nanotransducers. Nat Med 18(10):1580–1585. doi:10.1038/nm.2933
20. Wang X, Zhuang J, Peng Q, Li Y (2005) A general strategy for nanocrystal synthesis. Nature 437(7055):121–124. doi:10.1038/nature03968
21. Mai HX, Zhang YW, Si R, Yan ZG, Sun LD, You LP, Yan CH (2006) High-quality sodium rare-earth fluoride nanocrystals: controlled synthesis and optical properties. J Am Chem Soc 128(19):6426–6436. doi:10.1021/ja060212h
22. Boyer JC, Cuccia LA, Capobianco JA (2007) Synthesis of colloidal upconverting NaYF4:Er3+/Yb3+ and Tm3+/Yb3+ monodisperse nanocrystals. Nano Lett 7(3):847–852. doi:10.1021/nl070235+
23. Qian HS, Zhang Y (2008) Synthesis of hexagonal-phase core-shell NaYF4 nanocrystals with tunable upconversion fluorescence. Langmuir 24(21):12123–12125. doi:10.1021/la802343f
24. Li Z, Zhang Y (2008) An efficient and user-friendly method for the synthesis of hexagonal-phase NaYF(4):Yb, Er/Tm nanocrystals with controllable shape and upconversion fluorescence. Nanotechnology 19(34):345606. doi:10.1088/0957-4484/19/34/345606
25. Choi HS, Liu W, Liu F, Nasr K, Misra P, Bawendi MG, Frangioni JV (2010) Design considerations for tumour-targeted nanoparticles. Nat Nanotechnol 5(1):42–47. doi:10.1038/nnano.2009.314
26. Choi HS, Liu W, Misra P, Tanaka E, Zimmer JP, Itty Ipe B, Bawendi MG, Frangioni JV (2007) Renal clearance of quantum dots. Nat Biotechnol 25(10):1165–1170. doi:10.1038/nbt1340

27. Boyer JC, van Veggel FC (2010) Absolute quantum yield measurements of colloidal NaYF4:Er3+, Yb3+ upconverting nanoparticles. Nanoscale 2(8):1417–1419. doi:10.1039/c0nr00253d
28. Wang F, Han Y, Lim CS, Lu YH, Wang J, Xu J, Chen HY, Zhang C, Hong MH, Liu XG (2010) Simultaneous phase and size control of upconversion nanocrystals through lanthanide doping. Nature 463(7284):1061–1065. doi:10.1038/Nature08777
29. Liu Q, Sun Y, Yang T, Feng W, Li C, Li F (2011) Sub-10 nm hexagonal lanthanide-doped NaLuF4 upconversion nanocrystals for sensitive bioimaging in vivo. J Am Chem Soc 133(43):17122–17125. doi:10.1021/ja207078s
30. Wang F, Wang J, Liu X (2010) Direct evidence of a surface quenching effect on size-dependent luminescence of upconversion nanoparticles. Angew Chem Int Ed 49(41):7456–7460. doi:10.1002/anie.201003959
31. Chen Y, Gao Y, Chen H, Zeng D, Li Y, Zheng Y, Li F, Ji X, Wang X, Chen F, He Q, Zhang L, Shi J (2012) Engineering inorganic nanoemulsions/nanoliposomes by fluoride-silica chemistry for efficient delivery/co-delivery of hydrophobic agents. Adv Funct Mater:n/a-n/a. doi:10.1002/adfm.201102052
32. Ostrowski AD, Chan EM, Gargas DJ, Katz EM, Han G, Schuck PJ, Milliron DJ, Cohen BE (2012) Controlled synthesis and single-particle imaging of bright, sub-10 nm lanthanide-doped upconverting nanocrystals. ACS Nano 6(3):2686–2692. doi:10.1021/nn3000737
33. Bogdan N, Vetrone F, Ozin GA, Capobianco JA (2011) Synthesis of ligand-free colloidally stable water dispersible brightly luminescent lanthanide-doped upconverting nanoparticles. Nano Lett 11(2):835–840. doi:10.1021/nl1041929
34. Zhang T, Ge J, Hu Y, Yin Y (2007) A general approach for transferring hydrophobic nanocrystals into water. Nano Lett 7(10):3203–3207. doi:10.1021/nl071928t
35. Chen Z, Chen H, Hu H, Yu M, Li F, Zhang Q, Zhou Z, Yi T, Huang C (2008) Versatile synthesis strategy for carboxylic acid-functionalized upconverting nanophosphors as biological labels. J Am Chem Soc 130(10):3023–3029. doi:10.1021/ja076151k
36. Wang L, Yan R, Huo Z, Wang L, Zeng J, Bao J, Wang X, Peng Q, Li Y (2005) Fluorescence resonant energy transfer biosensor based on upconversion-luminescent nanoparticles. Angew Chem Int Ed 44(37):6054–6057. doi:10.1002/anie.200501907
37. Li LL, Zhang R, Yin L, Zheng K, Qin W, Selvin PR, Lu Y (2012) Biomimetic surface engineering of lanthanide-doped upconversion nanoparticles as versatile bioprobes. Angew Chem Int Ed 51(25):6121–6125. doi:10.1002/anie.201109156
38. Liu Q, Li C, Yang T, Yi T, Li F (2010) "Drawing" upconversion nanophosphors into water through host-guest interaction. Chem Commun 46(30):5551–5553. doi:10.1039/c0cc01352h
39. Chen F, Zhang S, Bu W, Liu X, Chen Y, He Q, Zhu M, Zhang L, Zhou L, Peng W, Shi J (2010) A "neck-formation" strategy for an antiquenching magnetic/upconversion fluorescent bimodal cancer probe. Chemistry 16(37):11254–11260. doi:10.1002/chem.201000525
40. Nyk M, Kumar R, Ohulchanskyy TY, Bergey EJ, Prasad PN (2008) High contrast in vitro and in vivo photoluminescence bioimaging using near infrared to near infrared up-conversion in Tm3+ and Yb3+ doped fluoride nanophosphors. Nano Lett 8(11):3834–3838
41. Park YI, Kim HM, Kim JH, Moon KC, Yoo B, Lee KT, Lee N, Choi Y, Park W, Ling D, Na K, Moon WK, Choi SH, Park HS, Yoon SY, Suh YD, Lee SH, Hyeon T (2012) Theranostic probe based on lanthanide-doped nanoparticles for simultaneous in vivo dual-modal imaging and photodynamic therapy. Adv Mater 24(42):5755–5761. doi:10.1002/adma.201202433
42. Tian G, Gu Z, Zhou L, Yin W, Liu X, Yan L, Jin S, Ren W, Xing G, Li S, Zhao Y (2012) Mn2+ dopant-controlled synthesis of NaYF4:Yb/Er upconversion nanoparticles for in vivo imaging and drug delivery. Adv Mater 24(9):1226–1231. doi:10.1002/adma.201104741
43. Wang F, Deng R, Wang J, Wang Q, Han Y, Zhu H, Chen X, Liu X (2011) Tuning upconversion through energy migration in core-shell nanoparticles. Nat Mater 10(12):968–973. doi:10.1038/nmat3149
44. Wang J, Wang F, Wang C, Liu Z, Liu X (2011) Single-band upconversion emission in lanthanide-doped KMnF3 nanocrystals. Angew Chem Int Ed 50(44):10369–10372. doi:10.1002/anie.201104192

45. Wang F, Liu X (2008) Upconversion multicolor fine-tuning: visible to near-infrared emission from lanthanide-doped NaYF4 nanoparticles. J Am Chem Soc 130(17):5642–5643. doi:10.1021/ja800868a
46. Chen G, Ohulchanskyy TY, Kumar R, Agren H, Prasad PN (2010) Ultrasmall monodisperse NaYF(4):Yb(3+)/Tm(3+) nanocrystals with enhanced near-infrared to near-infrared upconversion photoluminescence. ACS Nano 4(6):3163–3168. doi:10.1021/nn100457j
47. Dong C, Korinek A, Blasiak B, Tomanek B, van Veggel FCJM (2012) Cation exchange: a facile method to make NaYF4:Yb, Tm-NaGdF4Core–shell nanoparticles with a thin, tunable, and uniform shell. Chem Mater 24(7):1297–1305. doi:10.1021/cm2036844
48. Johnson NJ, Korinek A, Dong C, van Veggel FC (2012) Self-focusing by Ostwald ripening: a strategy for layer-by-layer epitaxial growth on upconverting nanocrystals. J Am Chem Soc 134(27):11068–11071. doi:10.1021/ja302717u
49. Chen G, Shen J, Ohulchanskyy TY, Patel NJ, Kutikov A, Li Z, Song J, Pandey RK, Agren H, Prasad PN, Han G (2012) (alpha-NaYbF4:Tm(3+))/CaF2 core/shell nanoparticles with efficient near-infrared to near-infrared upconversion for high-contrast deep tissue bioimaging. ACS Nano 6(9):8280–8287. doi:10.1021/nn302972r
50. Xie MY, Peng XN, Fu XF, Zhang JJ, Lia GL, Yu XF (2009) Synthesis of Yb3+/Er3+ co-doped MnF2 nanocrystals with bright red up-converted fluorescence. Scripta Mater 60(3):190–193. doi:10.1016/j.scriptamat.2008.10.010
51. Zeng JH, Xie T, Li ZH, Li YD (2007) Monodispersed nanocrystalline fluoroperovskite up-conversion phosphors. Cryst Growth Des 7(12):2774–2777. doi:10.1021/Cg070477n
52. Cai W, Hong H (2011) Peptoid and positron emission tomography: an appealing combination. Am J Nucl Med Mol Imaging 1(1):76–79
53. Cai W, Zhang Y, Kamp TJ (2011) Imaging of induced pluripotent stem cells: from cellular reprogramming to transplantation. Am J Nucl Med Mol Imaging 1(1):18–28
54. Zhang Y, Cai W (2012) Molecular imaging of insulin-like growth factor 1 receptor in cancer. Am J Nucl Med Mol Imaging 2(2):248–259
55. Zhang Y, Hong H, Engle JW, Yang Y, Barnhart TE, Cai W (2012) Positron emission tomography and near-infrared fluorescence imaging of vascular endothelial growth factor with dual-labeled bevacizumab. Am J Nucl Med Mol Imaging 2(1):1–13
56. Xia A, Gao Y, Zhou J, Li C, Yang T, Wu D, Wu L, Li F (2011) Core-shell NaYF4:Yb3+, Tm3+@FexOy nanocrystals for dual-modality T2-enhanced magnetic resonance and NIR-to-NIR upconversion luminescent imaging of small-animal lymphatic node. Biomaterials 32(29):7200–7208. doi:10.1016/j.biomaterials.2011.05.094
57. Guo H, Li Z, Qian H, Hu Y, Muhammad IN (2010) Seed-mediated synthesis of NaY F4:Y b, Er/NaGdF4 nanocrystals with improved upconversion fluorescence and MR relaxivity. Nanotechnology 21(12):125602. doi:10.1088/0957-4484/21/12/125602
58. Johnson NJJ, Oakden W, Stanisz GJ, Scott Prosser R, van Veggel FCJM (2011) Size-Tunable, Ultrasmall NaGdF4 Nanoparticles: Insights into Their T1 MRI Contrast Enhancement. Chemistry of Materials 23(16):3714–3722. doi:10.1021/cm201297x
59. Chen F, Bu W, Zhang S, Liu J, Fan W, Zhou L, Peng W, Shi J (2013) Gd3+-Ion-Doped Upconversion Nanoprobes: Relaxivity Mechanism Probing and Sensitivity Optimization. Adv Funct Mater 23(3):298–307. doi:10.1002/adfm.201201469
60. Xing H, Bu W, Zhang S, Zheng X, Li M, Chen F, He Q, Zhou L, Peng W, Hua Y, Shi J (2012) Multifunctional nanoprobes for upconversion fluorescence, MR and CT trimodal imaging. Biomaterials 33(4):1079–1089. doi:10.1016/j.biomaterials.2011.10.039
61. Xia A, Chen M, Gao Y, Wu D, Feng W, Li F (2012) Gd3+ complex-modified NaLuF4-based upconversion nanophosphors for trimodality imaging of NIR-to-NIR upconversion luminescence, X-Ray computed tomography and magnetic resonance. Biomaterials 33(21):5394–5405. doi:10.1016/j.biomaterials.2012.04.025
62. Zhou J, Zhu X, Chen M, Sun Y, Li F (2012) Water-stable NaLuF4-based upconversion nanophosphors with long-term validity for multimodal lymphatic imaging. Biomaterials 33(26):6201–6210. doi:10.1016/j.biomaterials.2012.05.036

63. Liu Y, Ai K, Liu J, Yuan Q, He Y, Lu L (2012) Hybrid BaYbF(5) nanoparticles: novel binary contrast agent for high-resolution in vivo X-ray computed tomography angiography. Adv Healthc Mater 1(4):461–466. doi:10.1002/adhm.201200028
64. Zeng S, Tsang MK, Chan CF, Wong KL, Hao J (2012) PEG modified BaGdF(5):Yb/Er nanoprobes for multi-modal upconversion fluorescent, in vivo X-ray computed tomography and biomagnetic imaging. Biomaterials 33(36):9232–9238. doi:10.1016/j.biomaterials.2012.09.019
65. Xiao Q, Bu W, Ren Q, Zhang S, Xing H, Chen F, Li M, Zheng X, Hua Y, Zhou L, Peng W, Qu H, Wang Z, Zhao K, Shi J (2012) Radiopaque fluorescence-transparent TaOx decorated upconversion nanophosphors for in vivo CT/MR/UCL trimodal imaging. Biomaterials 33(30):7530–7539. doi:10.1016/j.biomaterials.2012.06.028
66. Liu Q, Sun Y, Li C, Zhou J, Li C, Yang T, Zhang X, Yi T, Wu D, Li F (2011) 18F-Labeled magnetic-upconversion nanophosphors via rare-Earth cation-assisted ligand assembly. ACS Nano 5(4):3146–3157. doi:10.1021/nn200298y
67. Sun Y, Yu M, Liang S, Zhang Y, Li C, Mou T, Yang W, Zhang X, Li B, Huang C, Li F (2011) Fluorine-18 labeled rare-earth nanoparticles for positron emission tomography (PET) imaging of sentinel lymph node. Biomaterials 32(11):2999–3007. doi:10.1016/j.biomaterials.2011.01.011
68. Chen F, Bu W, Zhang S, Liu X, Liu J, Xing H, Xiao Q, Zhou L, Peng W, Wang L, Shi J (2011) Positive and negative lattice shielding effects co-existing in Gd(III) ion doped bifunctional upconversion nanoprobes. Adv Funct Mater 21(22):4285–4294. doi:10.1002/adfm.201101663
69. Liu Q, Chen M, Sun Y, Chen G, Yang T, Gao Y, Zhang X, Li F (2011) Multifunctional rare-earth self-assembled nanosystem for tri-modal upconversion luminescence/fluorescence/positron emission tomography imaging. Biomaterials 32(32):8243–8253. doi:10.1016/j.biomaterials.2011.07.053
70. Sun Y, Liu Q, Peng J, Feng W, Zhang Y, Yang P, Li F (2012) Radioisotope post-labeling upconversion nanophosphors for in vivo quantitative tracking. Biomaterials 27(12):01306–01303 01306. doi:10.1016/j.biomaterials.2012.11.047
71. Yang Y, Sun Y, Cao T, Peng J, Liu Y, Wu Y, Feng W, Zhang Y, Li F (2013) Hydrothermal synthesis of NaLuF4:153Sm, Yb, Tm nanoparticles and their application in dual-modality upconversion luminescence and SPECT bioimaging. Biomaterials 34(3):774–783
72. Cui S, Yin D, Chen Y, Di Y, Chen H, Ma Y, Achilefu S, Gu Y (2012) In vivo targeted deep-tissue photodynamic therapy based on near-infrared light triggered upconversion nanoconstruct. ACS Nano. doi:10.1021/nn304872n
73. Qian HS, Guo HC, Ho PC, Mahendran R, Zhang Y (2009) Mesoporous-silica-coated up-conversion fluorescent nanoparticles for photodynamic therapy. Small 5(20):2285–2290. doi:10.1002/smll.200900692
74. Zhao Z, Han Y, Lin C, Hu D, Wang F, Chen X, Chen Z, Zheng N (2012) Multifunctional core-shell upconverting nanoparticles for imaging and photodynamic therapy of liver cancer cells. Chem Asian J 7(4):830–837. doi:10.1002/asia.201100879
75. Chen F, Zhang S, Bu W, Chen Y, Xiao Q, Liu J, Xing H, Zhou L, Peng W, Shi J (2012) A uniform sub-50 nm-sized magnetic/upconversion fluorescent bimodal imaging agent capable of generating singlet oxygen by using a 980 nm laser. Chemistry 18(23):7082–7090. doi:10.1002/chem.201103611
76. Zhang P, Steelant W, Kumar M, Scholfield M (2007) Versatile photosensitizers for photodynamic therapy at infrared excitation. J Am Chem Soc 129(15):4526–4527. doi:10.1021/ja0700707
77. Meng H, Xue M, Xia T, Ji Z, Tarn DY, Zink JI, Nel AE (2011) Use of size and a copolymer design feature to improve the biodistribution and the enhanced permeability and retention effect of doxorubicin-loaded mesoporous silica nanoparticles in a murine xenograft tumor model. ACS Nano 5(5):4131–4144. doi:10.1021/nn200809t
78. Shan JN, Budijono SJ, Hu GH, Yao N, Kang YB, Ju YG, Prud'homme RK (2011) Pegylated composite nanoparticles containing upconverting phosphors and meso-tetraphenyl porphine

(TPP) for photodynamic therapy. Adv Funct Mater 21(13):2488–2495. doi:10.1002/adfm.201002516
79. Liu JN, Bu W, Pan LM, Zhang S, Chen F, Zhou L, Zhao KL, Peng W, Shi J (2012) Simultaneous nuclear imaging and intranuclear drug delivery by nuclear-targeted multifunctional upconversion nanoprobes. Biomaterials 33(29):7282–7290. doi:10.1016/j.biomaterials.2012.06.035
80. Wang C, Cheng L, Liu Z (2011) Drug delivery with upconversion nanoparticles for multi-functional targeted cancer cell imaging and therapy. Biomaterials 32(4):1110–1120. doi:10.1016/j.biomaterials.2010.09.069
81. Wang C, Tao H, Cheng L, Liu Z (2011) Near-infrared light induced in vivo photodynamic therapy of cancer based on upconversion nanoparticles. Biomaterials 32(26):6145–6154. doi:10.1016/j.biomaterials.2011.05.007
82. Chatterjee DK, Yong Z (2008) Upconverting nanoparticles as nanotransducers for photodynamic therapy in cancer cells. Nanomedicine 3(1):73–82. doi:10.2217/17435889.3.1.73
83. Xu H, Cheng L, Wang C, Ma X, Li Y, Liu Z (2011) Polymer encapsulated upconversion nanoparticle/iron oxide nanocomposites for multimodal imaging and magnetic targeted drug delivery. Biomaterials 32(35):9364–9373. doi:10.1016/j.biomaterials.2011.08.053
84. Cheng L, Yang K, Li Y, Chen J, Wang C, Shao M, Lee ST, Liu Z (2011) Facile preparation of multifunctional upconversion nanoprobes for multimodal imaging and dual-targeted photothermal therapy. Angew Chem Int Ed 50(32):7385–7390. doi:10.1002/anie.201101447
85. Ungun B, Prud'homme RK, Budijon SJ, Shan J, Lim SF, Ju Y, Austin R (2009) Nanofabricated upconversion nanoparticles for photodynamic therapy. Opt Express 17(1):80–86
86. Nichols JW, Bae YH (2012) Odyssey of a cancer nanoparticle: from injection site to site of action. Nano Today 7(6):606–618. doi:10.1016/j.nantod.2012.10.010
87. Zhang F, Braun GB, Pallaoro A, Zhang Y, Shi Y, Cui D, Moskovits M, Zhao D, Stucky GD (2012) Mesoporous multifunctional upconversion luminescent and magnetic "nanorattle" materials for targeted chemotherapy. Nano Lett 12(1):61–67. doi:10.1021/nl202949y